Journal of Biomechanics 93 (2019) 77–85

Contents lists available at ScienceDirect

Journal of Biomechanics

journal homepage: www.elsevier.com/locate/jbiomech
www.JBiomech.com

Investigation of left heart flow using a numerical correlation to model heart wall motion

Reza Samian [a,1], Maysam Saidi [b,*]

[a] Energy Research Center, Amirkabir University of Technology, Tehran, Iran
[b] Department of Mechanical Engineering, Faculty of Engineering, Razi University, Kermanshah, Iran

ARTICLE INFO

Article history:
Accepted 14 June 2019

Keywords:
CFD
Correlation
Dynamic mesh
Heart
Large eddy simulation
Wall movement

ABSTRACT

A three-dimensional computational fluid dynamics (CFD) method has been developed to model the flow in the left heart including atrium and ventricle. Since time resolution of the medical scans does not fit the requirements of the CFD calculations, the main challenge in a numerical simulation of heart chambers is wall motion modeling. This study employs a novel three-dimensional approximation scheme to correlate the wall boundary and grid movement in systole and diastole. It uses a geometry extracted from medical images in the literature and deformed based on the reported flow rates. The opening and closing of the mitral (MV) and the aortic valve (AV) considered as simultaneous events. Unstructured tetragonal grids were used for the meshing of the domain. The calculation was performed by a Navier–Stokes solver using the arbitrary Lagrange–Euler (ALE) formulation. Results show that the proposed correlation for the wall motion could predict the main features of heart flows.

1. Introduction

The cardiovascular disease (CVD) is a major cause of mortality in the world (Roth et al., 2017). Cardiac health is related to blood flow patterns in the human left ventricle (LV) (Wong et al., 2014; Khalafvand et al., 2018). Computational fluid dynamics (CFD) and fluid-structure interaction (FSI) have been widely used for the simulation and visualization of intraventricular flow (Baccani et al., 2002; Nakamura et al., 2003; Nguyen et al., 2015; Rossini et al., 2016; Su et al., 2016; Quarteroni et al., 2017; Doost et al., 2017; Gao et al., 2017; Liao et al., 2018). Zhong et al. (2018) reviewed challenges and opportunities in simulations of intra-cardiac flow.

The methods used to find the heart movements require spatial and temporal resolution, 4D-Echo provides high-speed resolution, which is especially useful when resolving the fast movements of structures. However, its low spatial resolution and image quality is difficult to use. On the other hand, methods such as CMR (Cardiac MRI) and CT (X-ray computed tomography) of the heart provide excellent spatial resolution, but their time resolution is orders-of-magnitude lower than the necessary temporal resolution for the flow simulation (Zhong et al., 2018). It could be inferred that a proper interpolation procedure for creating a CFD model is required for the simulation of the heart movement. This stage of the model is very difficult, and it is still an important challenge in the modeling of the patient's heart (Mittal et al., 2016). Either an interpolation method (Schenkel et al., 2009; Chnafa et al., 2014) or relying on a multi-beat acquisition (Mittal et al., 2016) is necessary for the simulation of the movement during the contraction-expansion cycle. In addition, for a useful application in medical routine, simulations must be possible with less computing time, which can perfectly be directed on local computing devices (Vellguth et al., 2018). Challenges due to the large-scale motion and complex deformation of the heart chambers make many current computational modeling of cardiac hemodynamics further away from clinical application (Mittal et al., 2016).

This manuscript tries to make CFD simulation applicable to clinical application. In this way it present a method to numerically simulate the heart without using of time-dependent series of medical images. Since that blood flow is incompressible, similar to Seo and Mittal (2013), heart chambers volumes are related to valve flows. Assuming a linear relation between volume change and myocardial motion, a time dependent position of heart wall is considered similar to time-dependent heart volume. Based on initial geometry, and time dependent heart wall position, the numerical simulation is performed and macroscopic flow features in heart extracted and compared with the literature. LA movement is also simulated to consider the atrial vortices which could influence the downstream ventricular flow.

* Corresponding author at: Razi University, Kermanshah 6714414971, Iran.
E-mail addresses: reza.samian@aut.ac.ir (R. Samian), msaidi@razi.ac.ir (M. Saidi).
[1] Amirkabir University of Technology, Tehran 1591634311, Iran.

https://doi.org/10.1016/j.jbiomech.2019.06.008
0021-9290/

2. Materials and methods

2.1. Cardiac physiology and numerical geometry

End-diastolic geometry is extracted from 3D medical images given by Chnafa et al. (2014). This is because: firstly, to compare the results with a paper which used the medical images in different times; secondly, the given geometry of simulated heart from different views which includes a scale of the geometry makes it possible to regenerate similar geometry; and thirdly, the values of valve flows gave us the opportunity to compare our results with the reference. Five cases with cell number of 396,733; 875,291; 3,004,224; 5,820,828; and 10,401,016 have been studied. Results have been reported based on the maximum cell number with the average mesh volume of 2.5e−811 m^3. The minimum and maximum volumes are 1.65e−12 m^3 and 1.79e−10 m^3, respectively. Fig. 1 depicts the numerical geometry of the left heart discretized with tetrahedral mesh, fluid mesh as well as a detailed view at the wall, and a plane section which divides the ventricle and aorta to two equal sections. This plane is used to report flow parameters in the following parts.

To ensure from the mesh independency of the results, a mesh study is performed by plotting velocity along the mitral centerline (a line from mitral center to apex) and average wall shear stress as shown in Fig. 2a and b, respectively. To quantify the difference of results, the normalized root mean square deviation (NRMSD) is computed:

$$NRMSD = \frac{\sqrt{\sum_{n=1}^{N}\left(Q_{1,n}-Q_{2,n}\right)^2}}{\frac{N}{Q_{max}-Q_{min}}}. \quad (1)$$

The result of the finest mesh differs less than 4% with the next fine one using NRMSD. By accepting 4% error, this mesh is selected.

Whereas in many experimental and numerical studies with constant diameter assumption of heart valves, real MV leaflets form a time-varying exit diameter D(t). However, it has been shown that the vortex formation time corresponding to the maxi-

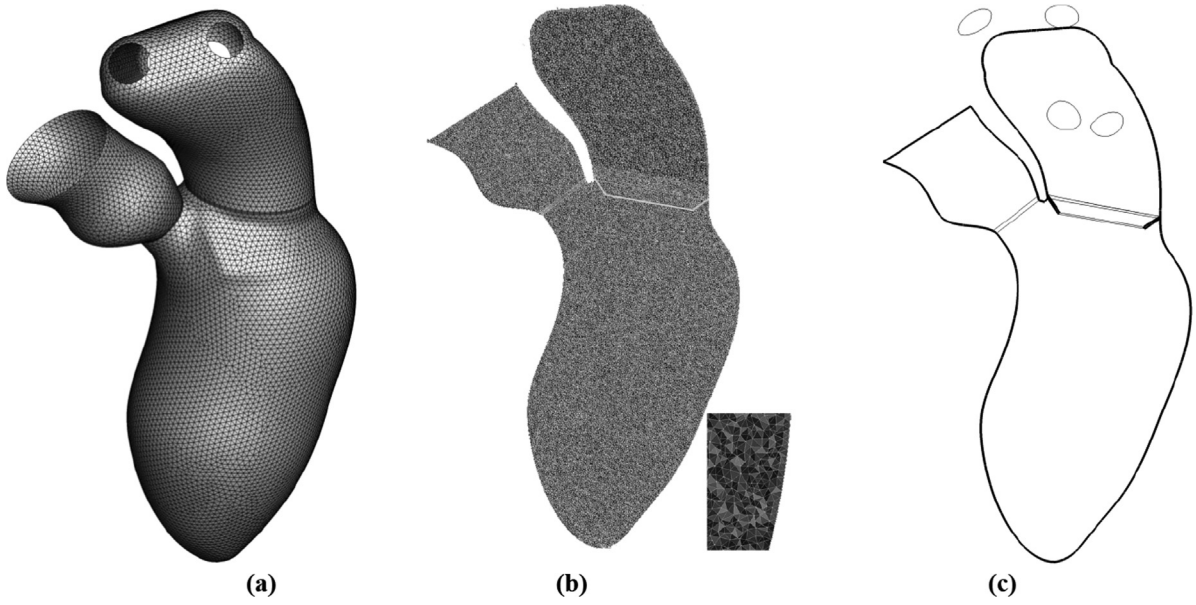

Fig. 1. Left side heart: (a) geometry and mesh (Cell No = 396,733), (b) fluid mesh (Cell No = 10,401,016) and detailed view at the wall, (c) plane section.

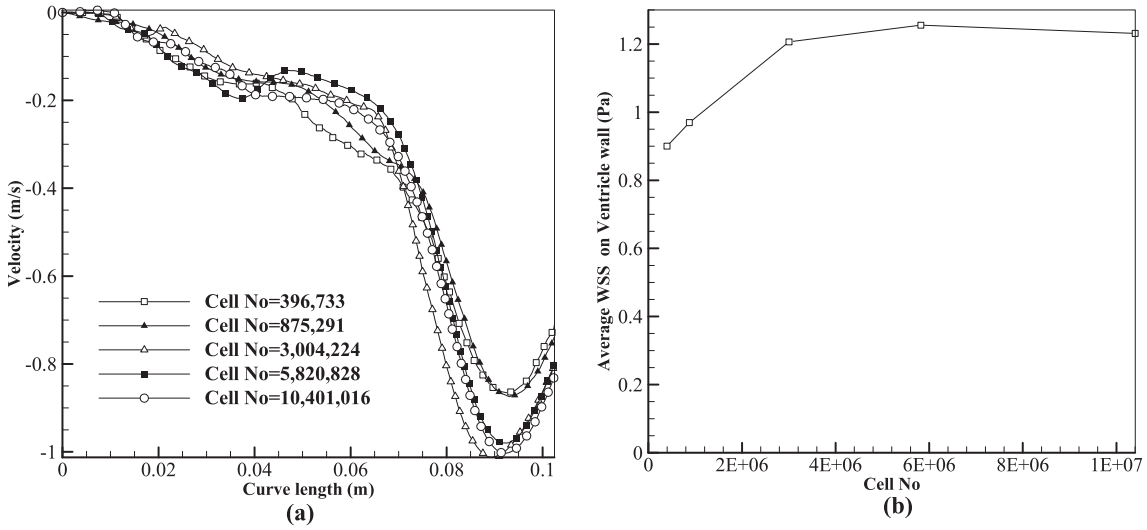

Fig. 2. Grid convergence (a) Instantaneous tangential-velocity profile along the mitral centerline at t/τ = 0.5 (b) Average WSS vs. cell number.

Table 1
Geometric characteristic of MV and AV.

	AV	MV
Diameter (mm)	16.782	25.232
Area (mm^2)	221.2	500.0

mum vortex growth remains unchanged (Gharib et al., 2006). In this paper, similar to most of the previous studies, the MV and AV diameters are assumed constant during the diastolic stage. The geometric characteristics of MV and AV are given in Table 1.

2.2. Governing equations and technical details

Mass and momentum conservation equations were solved using dynamic meshes in ANSYS Fluent 17.2. The details of solver settings are given in Table 2. In the present study, spring based smoothing method is used for the simulation of wall motion. In this method heart wall deforms according to the user-defined function that is applied to the myocardium wall while the internal edges between any two mesh nodes are idealized as a network of interconnected springs. More details are given in Fluent (2015). Since the boundary displacement is significant compared to the local cell sizes in current simulation, the cell quality may deteriorate or the cells may become degenerate. This could lead to negative volume, so re-meshing technique is used to decrease the mesh skewness.

The results have been considered after five cycles of the simulation to avoid the initial effects. The time step size used in the first five cycles was $t = 1 \times 10^{-3}$ s and then for the last cycle was switched to $t = 1 \times 10^{-4}$ s because of having Courant number less than 1. This Courant number is not mandatory for convergence but is better to be used for time accuracy of results. A computer with 32 GB RAM and 12 parallel threads of Core i7-4960X CPU was employed. The blood flowing in the heart chambers can be considered as homogeneous Newtonian fluid (Kitajima and Yoganathan, 2007). The density and dynamic viscosity are assumed constant equal to 1040 kg/m^3 and 0.00416 Pa s, respectively. While cardiac health is related to blood flow patterns including vortex ring in the human left ventricle, the visualization of intraventricular flow pattern needs choosing a method to capture the eddies properly. In the present work, the large eddy simulation (LES) approach is used which eddies smaller than filter size or mesh size are modeled and those greater than mesh size are resolved.

Table 2
Numerical solution setting.

Solver type		Pressure based
Pressure velocity coupling scheme		SIMPLE
Transient formulation		Second order implicit
Spatial discretization	Gradient	Least square cell based
	Pressure	Second order
	Momentum	Bounded central differencing

The sub-grid-scale stresses resulting from the filtering operation are unknown and require modeling. The sub-grid scales (SGS) are modeled using wall-adapting local eddy-viscosity (WALE) model and details are given in Fluent (2015).

2.3. Correlating cardiac cycle and numerical method

The initial and final stages of the heart cycle are considered and interval movement is obtained based on the blood flow in the heart valves and veins. Blood flow is incompressible, so the volume of heart ventricles and atriums is directly related to the valves flows. The volume of LV and LA can be written as follows:

$$V_a(t) = V_{a,d} + \int_0^t Q_{inlet}dt - \int_0^t Q_{mitral}dt, \tag{2}$$

$$V_v(t) = V_{v,d} + \int_0^t Q_{mitral}dt - \int_0^t Q_{Aorta}dt, \tag{3}$$

where $V_v(t)$ represents the volume of ventricle, $V_{v,d}$ is the end-diastolic volume of the ventricle, $V_{a,d}$ is the end diastolic volume of atrium, Q_{mitral} is the volumetric flow rate passing through MV from atrium to ventricle, Q_{Aorta} is the aortic flow rate which is pumped by LV to aorta, and Q_{inlet} is volumetric flow rate entering LA. The blood flow obtained from the work of Chnafa et al. (2014) is shown in Fig. 3. It includes Q_{inlet} named total heart inflow, Q_{mitral}, the flow passing through MV, and Q_{Aorta} which is the aortic flow.

The volumes changes are obtained by integration of volume flow rate differences and normalizing of ventricle and atrium volume changes. The normalized volume change of atrium $v_a^*(t)$ is defined as:

$$v_a^*(t) = \frac{V_a(t) - V_{a,d}}{V_{a,s} - V_{a,d}}, \tag{4}$$

where $V_{a,s}$ is the end-systolic volume of the atrium. The normalized volume change of ventricle $v_v^*(t)$ is defined as:

$$v_v^*(t) = \frac{V_v(t) - V_{v,s}}{V_{v,d} - V_{v,s}}, \tag{5}$$

where $V_{v,s}$ is the end-systolic volume of the ventricle. Now for the simulation of volumes movement, each heart period is composed of some expansions and contractions. Each motion is interpolated using a cosine form as the following formulation:

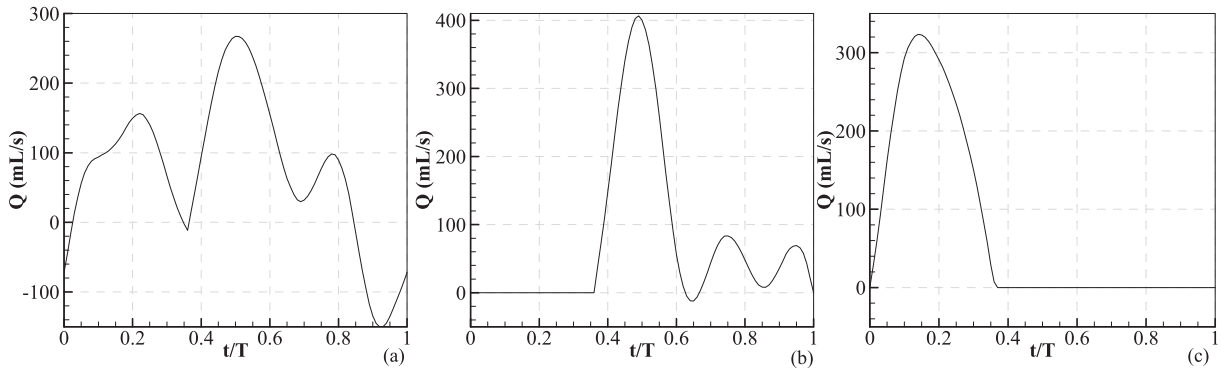

Fig. 3. (a) Total heart inflow from pulmonary veins, and flow rates passing from (b) MV and (c) AV in a heart cycle reported by Chnafa et al. (2014).

$$v(t) = \frac{(v_n + v_{n+1})}{2} + \frac{(v_n - v_{n+1})}{2} cos\left(\frac{t - t_n}{t_{n+1} - t_n}\pi\right), \quad t_n < t < t_{n+1} \tag{6}$$

where $v(t)$ is volume function used in wall motion definition, t is time, and subscript n represent a point which a new stage of expansion or contraction starts for the points shown in Fig. 4(a), and (b) for LA and LV, respectively.

Using this formulation for the simulation of heart movement the coefficients of $\frac{(v_n+v_{n+1})}{2}$ and $\frac{(v_n-v_{n+1})}{2}$ for the simulation of atrium and ventricle motions were used as listed in Tables 3 and 4.

After obtaining the movements of heart cavities, the formulation has been used for the simulation of heart wall movements. Since the movement of heart valves causes difficulty in simulation, a region around these valves is stationary and only heart cavities walls move with the mentioned formulation. Each point on the heart wall as shown in Fig. 5 fluctuates between end-diastolic (EDV) and end-systolic volumes (ESV). For example point LV1 at $t/\tau = 0$ reaches point LV2 at $t/\tau = 0.36$ and then returns to its initial point. In this simulation, a linear relation assumed between wall movement and volume changes so the normalized volume changes could be used directly as the normalized wall displacement formulation. To preserve the topology of surfaces and avoid creating singularities or self-intersections of the computational grids for large deformation, a central line inside chamber is selected which perpendicular lines from it to the surface of the chamber intersect the chamber at utmost one point. In other words, it means that all points on the wall could contract to this line cylindrically without self-intersection. In this work for the simplicity of the simulation, it is assumed that end-systolic points are located on a semi-conical shape. As a result, each heart cavity contracts toward this shape and then expands back to its initial position. Each point fluctuates from its maximum distance of the central line inside the cavity and the minimum radius of the cavity which is based on the flows reported in Chnafa et al. (2014).

2.4. Boundary conditions

The pulmonary veins and aortic orifice have been set as the domain inlet and outlet, respectively. While constant pressure equal to 666.6 Pa (5 mm Hg) is set for pulmonary veins as an inlet boundary condition, different pressures have been set for the aortic orifice during the systole and diastole which are 15998.7 and 10665.8 Pa (120 and 80 mm Hg), respectively. There is no direct way between the inlet and outlet during a heart cycle, so the flow results aren't related to the pressure difference between the inlet and outlet.

The time-position of the myocardial wall of the ventricle and atrium with no-slip boundary conditions are imposed as mentioned in the previous section. Since the valves have thin highly-moving structures, their precise movements are not extractable from MRI or CT scan exams (Chnafa et al., 2014), in this study they are assumed to switch between the open and closed positions for each valve.

Table 3
Parameters used for the simulation of LA.

n	t_n	v_n	$0.5(v_n + v_{n+1})$	$0.5(v_n - v_{n+1})$
0	0.03	0	0.5	−0.5
1	0.35	1	0.275	0.275
2	0.56	0.45	0.41	−0.14
3	0.69	0.73	0.285	0.015
4	0.76	0.7	0.265	−0.035
5	0.84	0.77	0.615	0.385

t_n: time of point which a new stage of expansion or contraction starts.
v_n: volume at time t_n.
v_{n+1}: volume at time t_{n+1}.

Table 4
Parameters used for the simulation of LV.

n	t_n	v_n	$0.5(v_n + v_{n+1})$	$0.5(v_n - v_{n+1})$
0	0	1	0.5	0.5
1	0.36	0	0.405	−0.405
2	0.63	0.81	0.805	0.005
3	0.67	0.8	0.86	−0.06
4	0.86	0.92	0.96	−0.04

t_n: time of point which a new stage of expansion or contraction starts.
v_n: volume at time t_n.
v_{n+1}: volume at time t_{n+1}.

3. Results

The left heart flows including the aortic flow, total heart inflow through pulmonary veins and mitral flows have been depicted in Fig. 6. In this study, the end-diastolic volume of the LV is 154 ml, and its end-systolic volume is 80 ml. It gives a stroke volume of

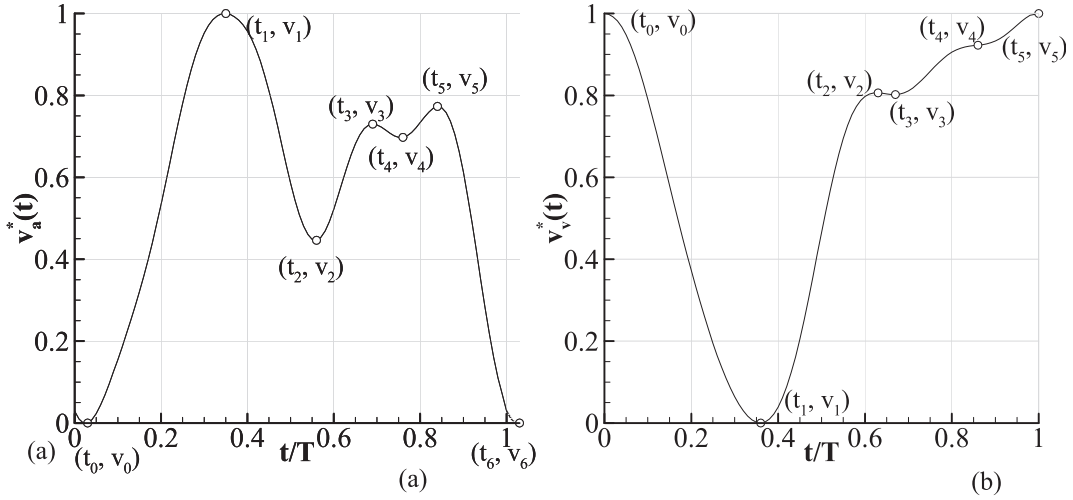

Fig. 4. Volume change during heart cycles based on Fig. 3 for left heart chambers (a) LA (b) LV.

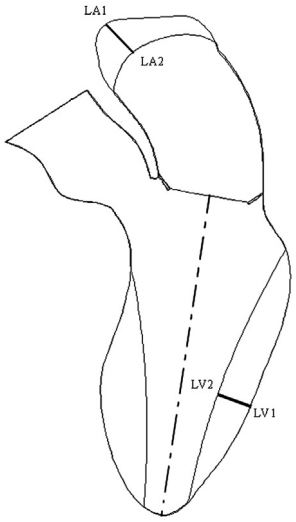

Fig. 5. Left heart chambers volume change.

74 ml or an ejection fraction of 48%. The end-systolic volume of the LA is 82 ml, and its minimum volume is 54 ml. The mitral flow rate shows three peaks: the first one during early diastolic filling is known as the E wave; the second one is a weak wave, and introduced as L wave by Chnafa et al. (2014); and the last one is known as A wave. The numerical procedure has followed the reported results well. According to Chnafa et al. (2014) the case belongs to a patient treated at the University Hospital of Toulouse Rangueil in France.

The velocity vectors in addition to velocity magnitude contours ranged from around 0.0 to 0.5 m/s in the central cross-section of the left heart are shown in Fig. 7 for $t/\tau = 0.1$ to 0.9. In the first three images, the MV is closed and blood is pumped into the aorta by ventricle compression. In $t/\tau = 0.4$ to 0.9, the AV is closed and blood enters from atrium through MV into the ventricle.

Fig. 8(a) depicts the vorticity magnitude contours ranged from 0 to 800 Hz at three different times. At $t/\tau = 0.1$ the MV is closed, and blood is pumped by ventricle contraction into the aorta. The friction of flow with the aorta valve generates high shear rate regions near the aorta valve wall.

Wall shear stress (WSS) contours near the walls are shown in Fig. 8(b) at times of 0.1, 0.5 and 0.8 of a cycle and the order of magnitude of maximum shear stress on walls decrease from 20 to 10 and 5 Pa, respectively.

Fig. 9 depicts the contour of normalized Q-criterion ranged from 0.1 to 0.5 to visualize the formation of vortex ring in E wave. In the vortex region, the pressure should be lower than the surrounding pressure. The flow of blood from the LA to the LV through the MV, known as the E wave, forms a rotating fluid mass called a mitral vortex ring (MVR) (Gharib et al., 2006). Development of a vortex ring needs pulsatility and a starting jet is ejecting to a quiescent flow could develop a vortex ring. The dimensionless measure of vortex formation time (VFT) is defined as (Kheradvar et al., 2012):

$$VFT = \frac{\bar{U}}{D}\delta T \tag{7}$$

where $\bar{U}$ is the mean velocity of jet, δT is the pulse duration, and D is the diameter of the MV.

$$VFT = \frac{\bar{U}}{D}\delta T = \frac{\bar{Q}/A}{D}\delta T = \frac{\bar{Q}}{AD}\delta T = \frac{\Delta V_v/\delta T}{AD}\delta T = 4\frac{\Delta V_v}{\pi D^3} \tag{8}$$

where $\bar{Q}$ is the average volume flow rate through MV, A is MV area, and D is MV diameter. In this simulation, the area of MV is $A = 500.0$ mm^2 and $D = 25.232$ mm. During the E wave, the volume change of ventricle is $\Delta V_v = 57$ ml. These values give $VFT = 4.5$ which is in the middle of normal range of 3.5–5.5 given by Kheradvar et al. (2012).

4. Discussion

In this paper an approach similar to method used by Taylor et al. (1996) and Seo and Mittal (2013) is incorporated for the simulation of heart wall movement according to the valve flows. In this method heart valve flows are integrated to obtain the heart cavities volumes versus time. Using time variation, the heart wall movement has been formulated, and the flow features during systole and diastole have been obtained. Assumed linear relation between volume change and myocardial motion makes it possible to use time-dependent heart volume chambers to define position of heart wall. Also left heart flows are obtained from experimental results given by Chnafa et al. (2014). In doing this work, a semi-conical shape is assumed as end-systolic geometry of LV. This assumption has been assumed based on end-systolic LV geometries given by Le and Sotiropoulos (2012) and Nguyen et al. (2015). Since the atrial vortices could influence the downstream ventricular flow, and the effect of abnormal LA is not negligible especially in the cases with high ejection fraction ratio (Su et al., 2019), LA movements is also simulated.

The reason behind the difference in valve flows with the Chnafa et al. (2014) could be listed as follow: firstly, the initial and final geometries are extracted from given images of the paper; secondly, the method used for the interpolation of heart chambers volumes data only considers extremum points which could generate error in the final result; and thirdly, a linear relation is assumed between volume change and wall movement.

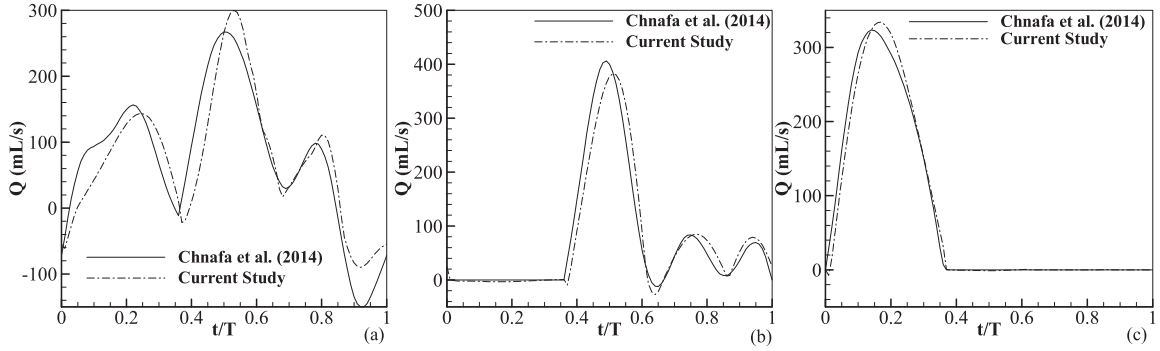

Fig. 6. (a) Total heart inflow from pulmonary veins, and flow rates passing from (b) MV and (c) AV in a heart cycle.

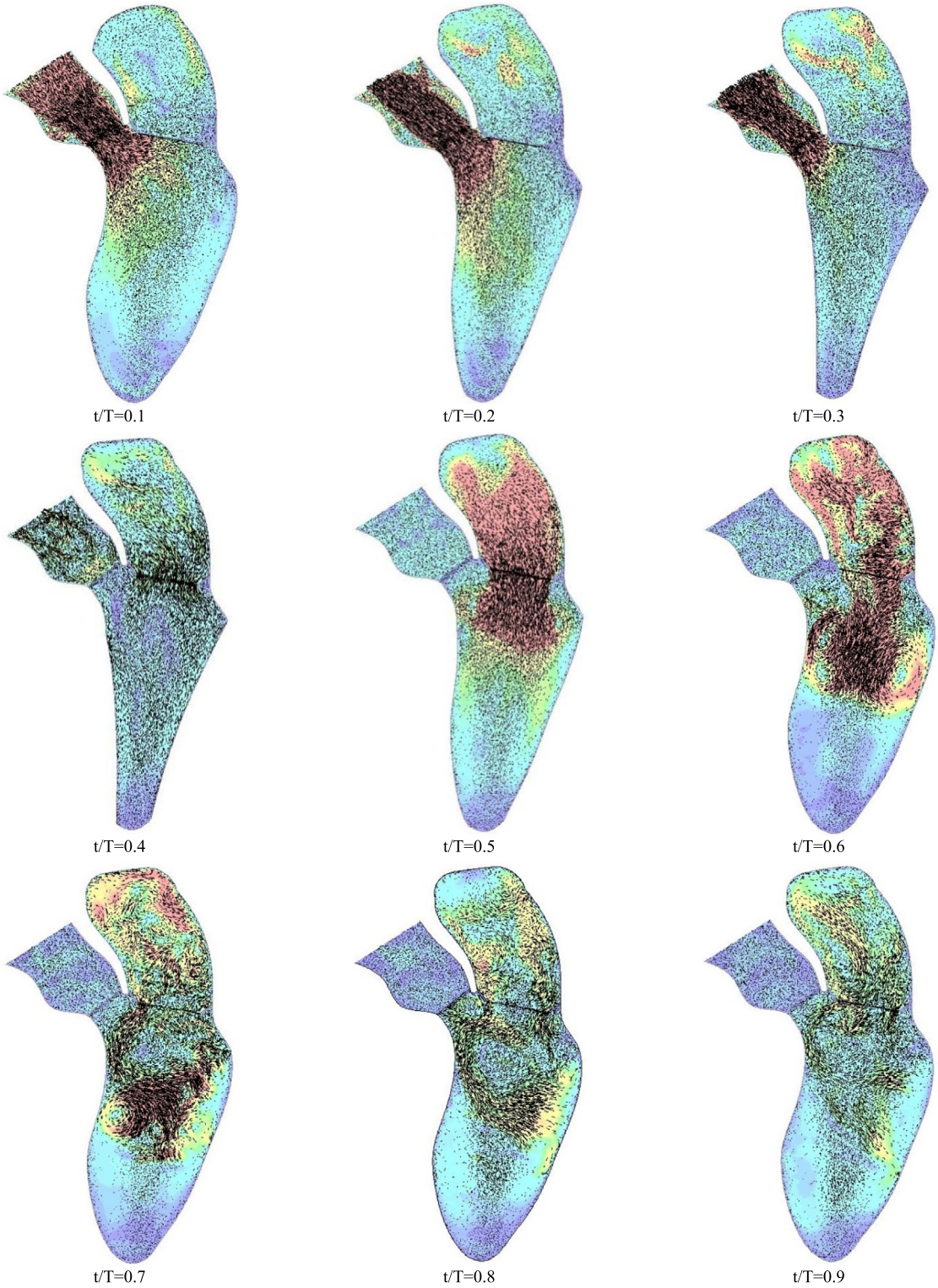

Fig. 7. Velocity vectors with velocity magnitude contour ranged from 0.0 to 0.5 m/s at different times (Velocities above 0.5 m/s are assigned red color). (For interpretation of the references to color in this figure legend, the reader is referred to the web version of this article.)

A vortex ring is shown to form at the tips of the mitral leaflets and propagates toward the myocardium wall. This phenomenon has been reported frequently in the past (Gharib et al., 2006; Toger et al., 2012; Chnafa et al., 2014, Vedula et al., 2016). During E wave a vortex ring formed after the MV at $t/\tau = 0.4$ because the LV wall expands and the lateral blood fills the place of the upward flow. The diastolic vortex rings show a significant role on the intra-ventricular flow (Bermejo et al., 2014). As can be seen in $t/\tau = 0.5$ since the ventricle wall moves rapidly it draws the blood with itself, and blood velocity has component normal to the ventricle wall. With time, irregular flow patterns including small and large vortices that encompass whole of the ventricle region are observed. It could be justified by the low flow from the mitral and the lack of considerable ventricle wall motion beside the great

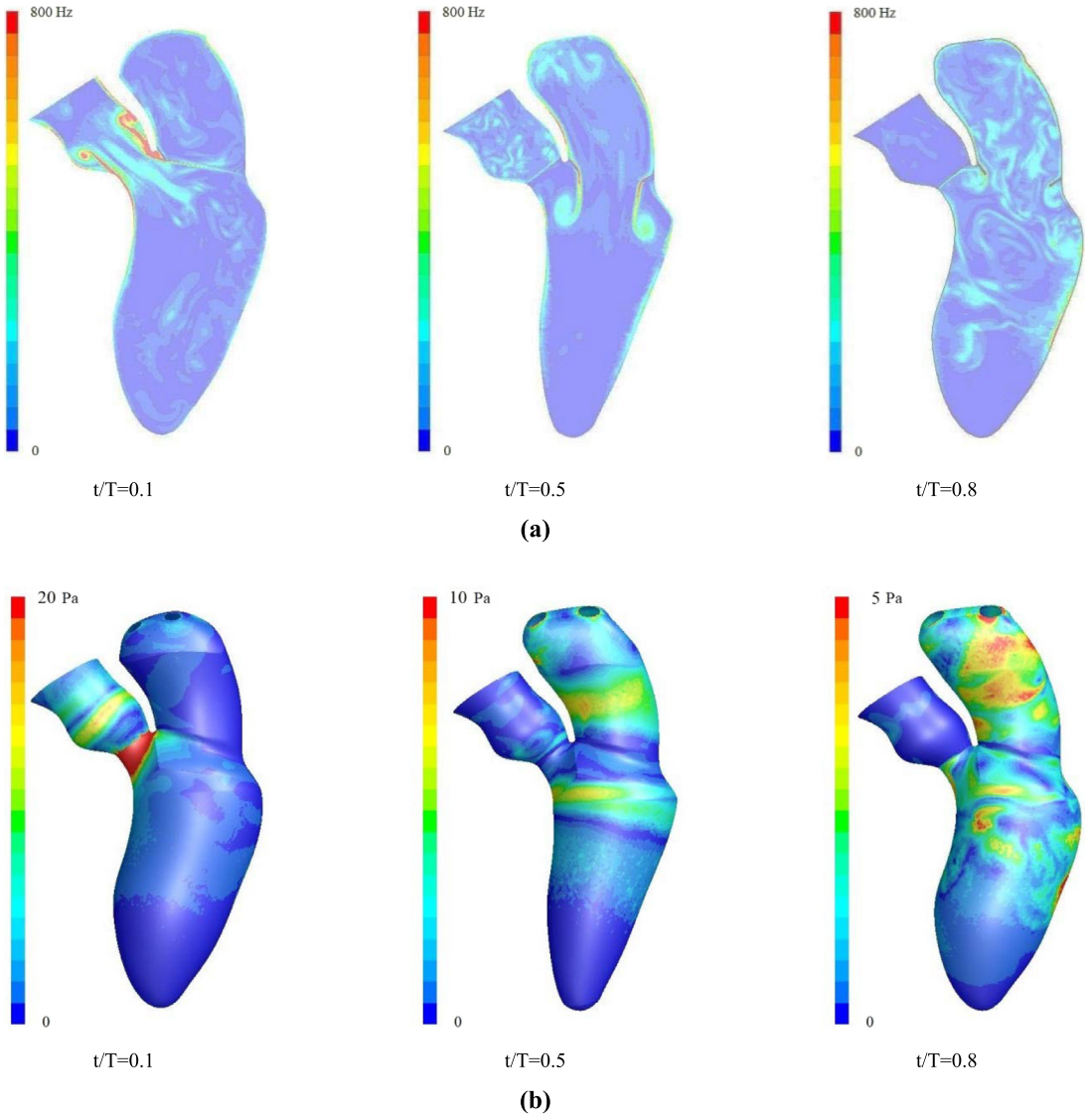

Fig. 8. Distribution of (a) vorticity and (b) Wall shear stress at different times.

momentum of the blood flow during the E wave. While Bermejo et al. (2014) suggest that vortex-flow interactions generate pressure forces inside the ventricle, Seo and Mittal (2013) suggest that the flow patterns themselves have not visible effect on the pumping function of the ventricle.

At diastole when the LV expands, and the MV is open, blood enters from the atrium through MV into the ventricle and forms a strong jet through the MV which is shown at $t/\tau = 0.5$. As the blood flows through the MV, the shear layer generates a vortex ring. At the final stages of the diastole, the flow is slow as can be seen at $t/\tau = 0.8$, so the high vortex regions distribute or disappear.

In an attempt to evaluate the effect of papillary muscles on flow feature Vedula et al. (2016) show that trabeculae significantly disrupt the vortices that formed during early diastole. However the main purpose of this study was introducing a method to capture the main macroscopic hemodynamic features in the left heart and thus the contours of WSS are simplified with limiting assumption of smooth wall for heart chambers.

At $t/\tau = 0.45$ to 0.60 during the early diastolic filling, the MVR formation at the edge of the mitral orifice and collapse of vortex ring can be seen in Fig. 9 which is in accordance with Le and Sotiropoulos (2012) with donut-shape vorticity distribution around the main ring circumference. There is not any ring vortex at time $t/\tau = 0.58$, 0.6, and 0.7. The main period of ring vortex generation was during E-wave. In vitro and in vivo studies have shown that a vortex ring rolls up during early diastole or E-wave (Kheradvar et al., 2012).

4.1. Novelty

While Chnafa et al. (2014) used geometry obtained from medical scans to generate surface and volume meshes for flow simulations in LV during a heart cycle, in this paper, an approach similar to method used by Taylor et al. (1996) and Seo and Mittal (2013) was used for interpolation of heart movement. In our method heart valve flows integrated to obtain heart cavities volumes by time. Using time variation, the heart wall movement has been formulated and the flow features during systole and diastole have been obtained. While large-scale motion and complex deformation of the heart chambers makes many current computational modeling of cardiac hemodynamics challenging and away from clinical application (Mittal et al., 2016), the given numerical procedure can simulate the left heart practically.

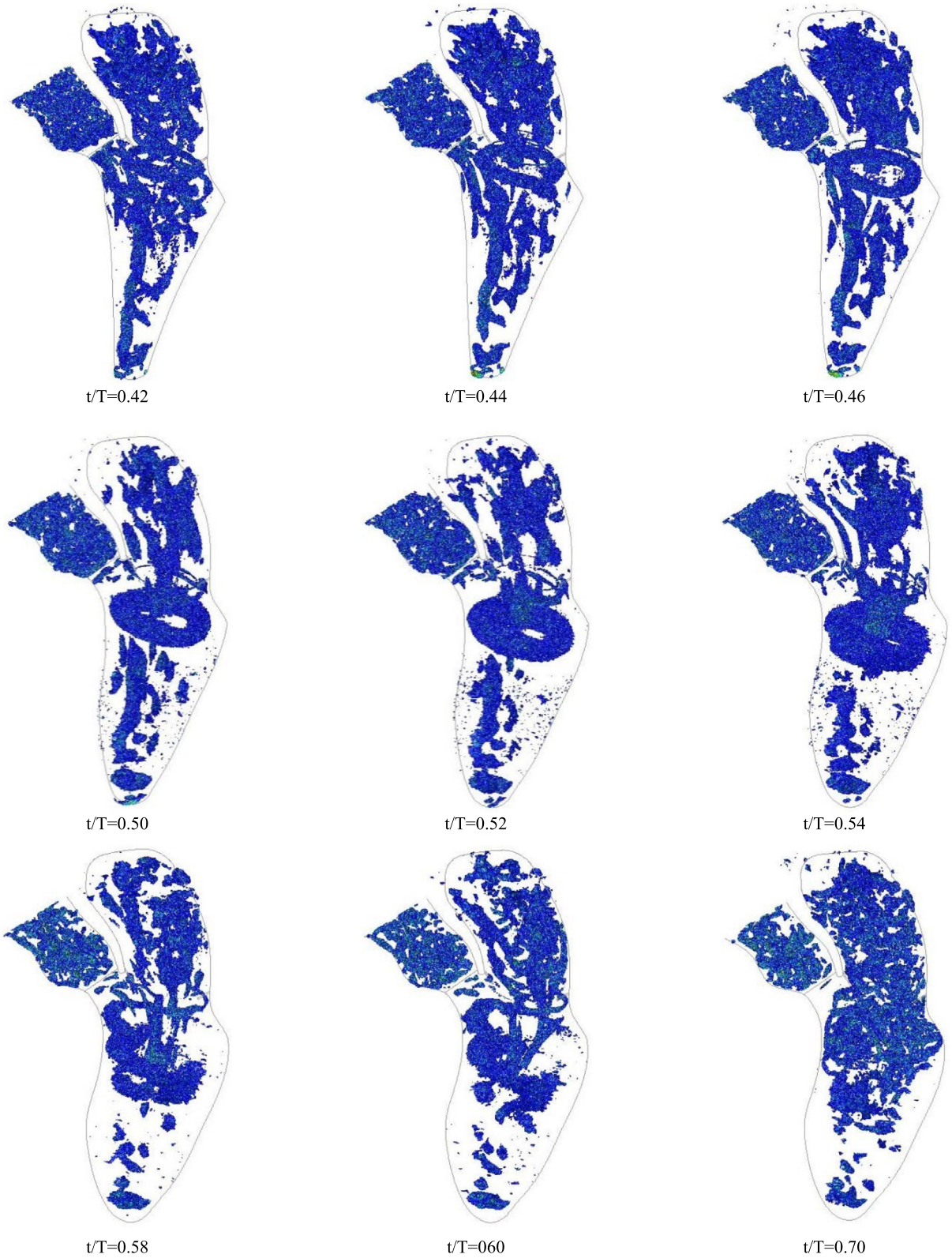

Fig. 9. Vortex formation and collapse visualization by normalized Q-criterion ranged from 0.1 to 0.5.

4.2. Limitations

A linear relation is assumed for volume change and myocardial wall motion. A similar assumption for volume change of a sphere shows less than 3% difference according this assumption. Since the closing time is short compared to whole heart cycle, the valves are assumed as instantaneous opening and closing in this study and a short-lasting portion of cardiac cycle i.e. isovolumetric contraction was not simulated in this study.

The end-systolic geometry is supposed as a semi-conical shape. It has been supposed based on end-systolic LV geometries given by Le and Sotiropoulos (2012) and Nguyen et al. (2015).

In this paper smooth walls are assumed for heart chambers and internal trabeculae features of walls have been neglected. This feature in one hand could enhance mixing and viscous dissipation, and on the other hand it could lead to localized regions of stagnation and recirculation (Seo and Mittal, 2013). In this simulation heart wall motions are assumed radially and twisting of the heart wall are neglected, although the method is capable to consider this feature to the simulation.

5. Conclusion

Important aspects of the physiological left heart including the entire ventricle and atrium, the aorta root, the pulmonary veins, and the valves have been modeled. The blood flow in the left heart conducted in a full heart cycle, so a variety of parameters in different times and locations are accessible. Velocity, vorticity, wall shear stress and vortex distributions allow investigating the effect of cardiovascular diseases on the heart hemodynamics.

The results show that the employed correlation is able to model the main features of interventricular heart flow. The mitral vortex ring, a feature of ventricle flow during the early diastolic filling, known as the E wave, has been captured and shown in velocity vectors as well as Q-criterion.

Declaration of Competing Interest

The authors have no conflicts of interest concern.

Appendix A. Supplementary material

Supplementary data to this article can be found online at https://doi.org/10.1016/j.jbiomech.2019.06.008.

References

Baccani, B., Domenichini, F., Pedrizzetti, G., Tonti, G., 2002. Fluid dynamics of the left ventricular filling in dilated cardiomyopathy. J. Biomech. 35 (5), 665–671.

Bermejo, J., Benito, Y., Alhama, M., Yotti, R., Martínez-Legazpi, P., Del Villar, C.P., Pérez-David, E., González-Mansilla, A., Santa-Marta, C., Barrio, A., Fernández-Avilés, F., 2014. Intraventricular vortex properties in nonischemic dilated cardiomyopathy. Am. J. Physiol.-Heart Circul. Physiol. 306 (5), H718–H729.

Chnafa, C., Mendez, S., Nicoud, F., 2014. Image-based large-eddy simulation in a realistic left heart. Comput. Fluids. 94, 173–187.

Doost, S.N., Zhong, L., Su, B., Morsi, Y.S., 2017. Two-dimensional intraventricular flow pattern visualization using the image-based computational fluid dynamics. Comput. Methods Biomech. Biomed. Eng. 20 (5), 492–507.

Fluent, A.N.S.Y.S., 2015. Theory guide. Ansys Inc..

Gharib, M., Rambod, E., Kheradvar, A., Sahn, D.J., Dabiri, J.O., 2006. Optimal vortex formation as an index of cardiac health. Proc. Natl. Acad. Sci. 103 (16), 6305–6308.

Gao, H., Feng, L., Qi, N., Berry, C., Griffith, B.E., Luo, X., 2017. A coupled mitral valve-left ventricle model with fluid–structure interaction. Med. Eng. Phys. 47, 128–136.

Kitajima, H., Yoganathan, A.P., 2007. Blood flow-the basics of the discipline. In: Fogel, M.A., (Ed.). Ventricular Function and Blood Flow in Congenital Heart Disease, https://doi.org/10.1002/9780470994849.ch3.

Khalafvand, S.S., Voorneveld, J.D., Muralidharan, A., Gijsen, F.J.H., Bosch, J.G., van Walsum, T., Haak, A., de Jong, N., Kenjeres, S., 2018. Assessment of human left ventricle flow using statistical shape modelling and computational fluid dynamics. J. Biomech. 74, 116–125.

Kheradvar, A., Assadi, R., Falahatpisheh, A., Sengupta, P.P., 2012. Assessment of transmitral vortex formation in patients with diastolic dysfunction. J. Am. Soc. Echocardiogr. 25 (2), 220–227.

Le, T.B., Sotiropoulos, F., 2012. On the three-dimensional vortical structure of early diastolic flow in a patient-specific left ventricle. Eur. J. Mech. B/Fluids. 35, 20–24.

Liao, S., Neidlin, M., Li, Z., Simpson, B., Gregory, S.D., 2018. Ventricular flow dynamics with varying LVAD inflow cannula lengths: In-silico evaluation in a multiscale model. J. Biomech. 72, 106–115.

Mittal, R., Seo, J.H., Vedula, V., Choi, Y.J., Liu, H., Huang, H.H., Jain, S., Younes, L., Abraham, T., George, R.T., 2016. Computational modeling of cardiac hemodynamics: Current status and future outlook. J. Comput. Phys. 305, 1065–1082.

Nakamura, M., Wada, S., Mikami, T., Kitabatake, A., Karino, T., 2003. Computational study on the evolution of an intraventricular vortical flow during early diastole for the interpretation of color M-mode Doppler echocardiograms. Biomech. Model. Mechanobiol. 2 (2), 59–72.

Nguyen, V.T., Wibowo, S.N., Leow, Y.A., Nguyen, H.H., Liang, Z., Leo, H.L., 2015. A patient-specific computational fluid dynamic model for hemodynamic analysis of left ventricle diastolic dysfunctions. Cardiovasc. Eng. Technol. 6 (4), 412–429.

Quarteroni, A., Lassila, T., Rossi, S., Ruiz-Baier, R., 2017. Integrated Heart—Coupling multiscale and multiphysics models for the simulation of the cardiac function. Comput. Methods Appl. Mech. Eng. 314, 345–407.

Rossini, L., Martinez-Legazpi, P., Vu, V., Fernández-Friera, L., del Villar, C.P., Rodríguez-López, S., Benito, Y., Borja, M.G., Pastor-Escuredo, D., Yotti, R., Ledesma-Carbayo, M.J., 2016. A clinical method for mapping and quantifying blood stasis in the left ventricle. J. Biomech. 49 (11), 2152–2161.

Roth, G.A., Johnson, C., Abajobir, A., Abd-Allah, F., Abera, S.F., Abyu, G., Ahmed, M., Aksut, B., Alam, T., Alam, K., Alla, F., 2017. Global, regional, and national burden of cardiovascular diseases for 10 causes, 1990 to 2015. J. Am. Coll. Cardiol., 23715

Schenkel, T., Malve, M., Reik, M., Markl, M., Jung, B., Oertel, H., 2009. MRI-based CFD analysis of flow in a human left ventricle: methodology and application to a healthy heart. Ann. Biomed. Eng. 37 (3), 503–515.

Seo, J.H., Mittal, R., 2013. Effect of diastolic flow patterns on the function of the left ventricle. Phys. Fluids. 25 (11), 110801.

Su, B., San Tan, R., Le Tan, J., Guo, K.W.Q., Zhang, J.M., Leng, S., Zhao, X., Allen, J.C., Zhong, L., 2016. Cardiac MRI based numerical modeling of left ventricular fluid dynamics with mitral valve incorporated. J. Biomech. 49 (7), 1199–1205.

Su, B., Wang, X., Kabinejadian, F., Chin, C., Le, T.T., Zhang, J.M., 2019. Effects of left atrium on intraventricular flow in numerical simulations. Comput. Biol. Med. 106, 46–53.

Taylor, T.W., Suga, H., Goto, Y., Okino, H., Yamaguchi, T., 1996. The effects of cardiac infarction on realistic three-dimensional left ventricular blood ejection. J. Biomech. Eng. 118 (1), 106–110.

Toger, J., Kanski, M., Carlsson, M., Kovacs, S.J., Soderlind, G., Arheden, H., Heiberg, E., 2012. Vortex ring formation in the left ventricle of the heart: analysis by 4D flow MRI and Lagrangian coherent structures. Ann. Biomed. Eng. 40 (12), 2652–2662.

Vedula, V., Seo, J.H., Lardo, A.C., Mittal, R., 2016. Effect of trabeculae and papillary muscles on the hemodynamics of the left ventricle. Theor. Comput. Fluid Dyn. 30 (1–2), 3–21.

Vellguth, K., Brüning, J., Goubergrits, L., Tautz, L., Hennemuth, A., Kertzscher, U., Degener, F., Kelm, M., Sündermann, S., Kuehne, T., 2018. Development of a modeling pipeline for the prediction of hemodynamic outcome after virtual mitral valve repair using image-based CFD. Int. J. Comp. Assis. Radiol. Surg. 13 (11), 1795–1805.

Wong, K., Samaroo, G., Ling, I., Dembitsky, W., Adamson, R., Del Alamo, J.C., May-Newman, K., 2014. Intraventricular flow patterns and stasis in the LVAD-assisted heart. J. Biomech. 47 (6), 1485–1494.

Zhong et al., 2018. Application of patient-specific computational fluid dynamics in coronary and intra-cardiac flow simulations: challenges and opportunities. Front. Physiol. 9, 742.